Catalysis Today 158 (2010) 215–219

Contents lists available at ScienceDirect

Catalysis Today

journal homepage: www.elsevier.com/locate/cattod

Effect of the calcination conditions on the NO_x storage behavior of the perovskite $BaFeO_{3-x}$ catalysts

Hui Xian[a], Xingwen Zhang[a], Xingang Li[a,*], Honghu Zou[a], Ming Meng[a,**], Zhiqiang Zou[a], Lihong Guo[b], Noritatsu Tsubaki[c,**]

[a] Tianjin Key Laboratory of Applied Catalysis Science and Technology, School of Chemical Engineering and Technology, Tianjin University, Weijin Road 92, Nankai District, Tianjin 300072, PR China
[b] School of Chemistry and Chemical Engineering, Henan University of Technology, Zhengzhou 450001, PR China
[c] Department of Applied Chemistry, School of Engineering, University of Toyama, Gofuku 3190, Toyama City, Toyama 930-8555, Japan

ARTICLE INFO

Article history:
Available online 9 April 2010

Keywords:
Perovskite
$BaFeO_{3-x}$
Lean-burn
NO_x storage
Noble metal free

ABSTRACT

The $BaFeO_{3-x}$ perovskite catalyst was prepared by sol–gel method for NO_x storage under lean-burn conditions. During the catalyst precursor calcination, a series of complex solid reactions happened, and the $BaCO_3$, formed during citric acid combustion, played a key role to react with the spinel species achieving the aimed perovskite. On the Ba–Fe–750F catalyst, the perovskite phase and the small amount of spinel phase were evidenced by XRD, and some well dispersed carbonate was also detected by FT-IR. Under lean-burn conditions, the NO_x was easily stored on the Ba–Fe–750F catalyst, and its optimized NO_x storage capacity (NSC), i.e. 333.5 $\mu mol\ g^{-1}$, was obtained at 400 °C. At above 400 °C, the stored nitrate became unstable and decomposed, resulting in the sharp decrease of NSC. Two kinds of the NO_x storage sites were identified by *in situ* DRIFTS experiments that the carbonate remaining on the catalyst could transform to monodentate nitrate, and the A site Ba in the perovskite structure could directly bind with NO_x to form N-bounded nitrate. This $BaFeO_{3-x}$ perovskite catalyst was a potential NO_x storage material with noble metal free.

© 2010 Elsevier B.V. All rights reserved.

1. Introduction

Lean-burn diesel and gasoline engines are widely applied in vehicles to reduce greenhouse effect and improve fuel economic efficiency [1]. NO_x storage-reduction (NSR) technique, which was firstly proposed by Toyota company [2], provides an potential route to reduce NO_x under lean-burn conditions. The NSR catalysts usually contain barium oxide and noble metals [2–4]. NO is firstly oxidized to NO_2 on the noble metal, and then is stored on the barium oxide nearby [4–6] under lean-burn atmosphere. The stored NO_x can be further reduced to N_2 by the reducing components in the exhaust gases, such as hydrocarbons and CO [2–4] under rich-burn atmosphere. Hao and co-workers reported one kind of hydrotalcite-like compounds, which were utilized for NO_x capture, decomposition and reduction [7,8]. Recently, the electrochemical catalysts, such as Pt–BaO/YSZ [9] and Pt–K/β-Al_2O_3 [10], are also developed to act as both NSR catalyst and sensor for the lean-rich cycles of the atmosphere in diesel engine.

Now, perovskite type catalysts in ABO_3 formula are broadly utilized in NO_x removal processes [11,12]. Their catalytic properties are mainly due to the abnormal valence of the B site element, which is induced by the electric neutrality principle. Perovskite oxides are deemed as potential substitutes for noble metals because of their prior redox properties, stable structures and low cost. Therefore, the perovskite type catalysts were ever evaluated for the NO_x storage process [4,13,14]. Hodjati et al. reported one kind of the perovskite catalyst that the A site element was Ba, Sr, or Ca to storage NO_x under the lean-burn conditions, and the B site element was Sn, Zr, or Ti. They found that the NO_x adsorption ability of the perovskite catalysts was in the order of Ba > Sr > Ca and Sn > Zr > Ti, and the $BaSnO_3$ catalyst possessed the best NO_x absorption ability [13]. However, when it was exposed in the mixture of SO_2 and NO_x, it was poisoned by sulfation quickly [15]. Yamazaki et al. found that the existence of Fe_2O_3 in the Pt/BaO/γ-Al_2O_3 catalyst improved significantly its sulfur resistance by inhibiting the growth in the size of the neighboring $BaSO_4$ and accelerating the decomposition of $BaSO_4$ under the reducing condition [16]. Casapu et al. studied the Pt/Ba/CeO_2 and Pt/Ba/Al_2O_3 catalysts [17,18]. They found the formation of the perovskite species $BaPtO_3$ and Ba_2PtCeO_6 increased the Pt dispersion on the support. Could the iron species be limited in the crystal lattice of the NSR perovskite catalyst to improve its sulfur-resistance by increasing iron dispersion? In our

* Corresponding author. Tel.: +86 22 27892275; fax: +86 22 27892275.
** Corresponding authors.
E-mail address: xingang_li@tju.edu.cn (X. Li).

0920-5861/$ – see front matter © 2010 Elsevier B.V. All rights reserved.
doi:10.1016/j.cattod.2010.03.026

previous work, a complex-oxide catalyst Ba–Fe–O containing perovskites, spinel, and carbonate species was shortly introduced, and it presented a good NO_x storage ability and an improved sulfur-resistance [19].

In this study, the perovskite type $BaFeO_{3-x}$ catalyst was prepared by sol–gel method, which was synthesized under the more severe preparation conditions than the previous study [19], such as the accurate pH value adjustment to the sol, the calcination procedure designed for the xerogel, and the continuous air flowing conditions during calcination to obtain a better perovskite structures. The perovskite formation process was determined by thermogravimetry (TG) and FT-IR. The structure property of the perovskite catalyst was characterized by XRD, and BET surface area measurement. The NO_x storage behavior over the perovskite catalysts were also investigated and clarified through the NO-TPD and *in situ* DRIFTS experiments.

2. Experimental

2.1. Catalyst preparation

The $BaFeO_{3-x}$ catalysts were prepared by sol–gel method. Briefly, the required amount of $Ba(NO_3)_2$ (Tianjin University, Kewei Co.) and $Fe(NO_3)_3{\cdot}9H_2O$ (Tianjin University, Kewei Co.) was dissolved together in diluted water to obtain 0.05 mol L^{-1} for each, and then the solution was ultrasonic-treated for 0.5 h, followed by addition of 0.05 mol L^{-1} of citric acid (CA, Tianjin University, Kewei Co.) solution. Meanwhile, the pH value of the aqueous solution kept at 9.0 with the adjustment of 28% $NH_3{\cdot}H_2O$ solution (Tianjin University, Kewei Co.), and the temperature of the aqueous solution was maintained at 80 °C. The molar ratio for each component was Ba:Fe:CA = 1:1:2. After vigorous stirring and evaporation, a transparent gel was formed, which was then dried at 120 °C overnight. The obtained xerogel precursor was firstly calcined from room temperature to 350 °C in air with a rate of 1 °C min^{-1}, stayed for 2 h to completely remove CA, and was then calcined at 750 °C for 6 h with a rate of 4 °C min^{-1}. The whole calcination process was conducted in a pipe furnace with the continuous air flow (50 mL min^{-1}) to eliminate the produced CO_2 during CA combustion. The catalyst was denoted as Ba–Fe–750F. Moreover, the catalysts prepared with the same precursor synthesis method and the same calcination procedure in static air, i.e. without air flow, with a muffle furnace were also compared with the Ba–Fe–750F catalyst. These catalysts were denoted as Ba–Fe–750S, Ba–Fe–850S, and Ba–Fe–950S, according to the different calcination temperature at 750, 850 and 950 °C for 6 h, respectively.

2.2. Catalyst characterizations

The thermogravimetry (TG) analysis was conducted with a Perkin-Elmer Diamond TG instrument. Approximate 30 mg of the precursor was used. It was implemented in an air flow of 100 mL min^{-1}. The temperature increased from room temperature to 900 °C at a rate of 10 °C min^{-1}.

For the FT-IR transmission spectroscopy experiment, a mixture of the sample and the vacuum-dried IR-grade KBr with a weight ratio of 1:100 was pressed into a disc, and then recorded with a Nexus FT-IR spectrometer apparatus (Thermo Nicolet Co.) equipped with a MCT detector using 64 scans and a resolution of 4 cm^{-1} in the range from 400 to 4000 cm^{-1}.

The X-ray diffraction (XRD) measurements were carried out on an X'pert pro rotatory diffractometer, using Co Kα (λ = 0.17890 nm) as radiation source. The X-ray tube was operated at 40 kV and 40 mA.

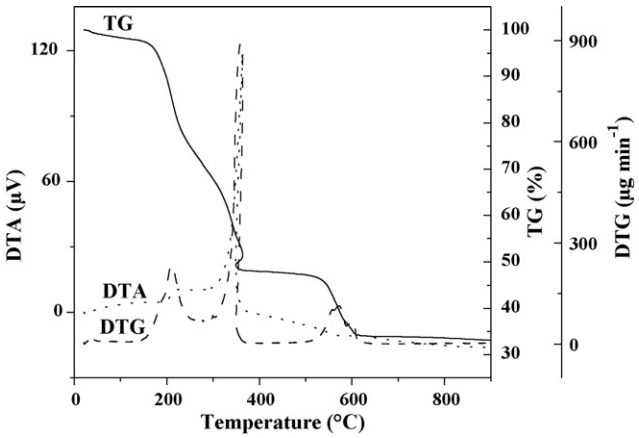

Fig. 1. TG profiles of the catalyst precursor: DTG (dash line), DTA (dot line), and TG (solid line).

The BET surface area of the catalysts was determined by N_2 physisorption using an automatic gas adsorption system (NOVA 2000, Quantachrome Co.) at −196 °C. The sample was outgassed at 300 °C for 8 h prior to N_2 physisorption.

The *in situ* Diffuse Reflectance Infrared Fourier Transform Spectroscopy (DRIFTS) experiments were carried out on the same Nexus FT-IR spectrometer as the FT-IR transmission spectroscopy experiments with 32 scans. For the NO_x sorption experiment at 400 °C with the various NO_x sorption period, the catalyst was pretreated in 5% O_2/He at 400 °C for 30 min to record the background spectrum, and then 800 ppm NO and 5% O_2 diluted by He was introduced to the sample cell. The spectra were collected at the different exposure time from 1 to 60 min. The flow rate of the introduced gas for all of the DRIFTS experiments was 50 mL min^{-1}.

2.3. NO_x sorption process

The NO_x storage capacity (NSC) measurements were carried out in a conventional fixed bed quartz reactor (i.d. = 8 mm) under atmospheric pressure. 0.5 g of the catalyst was used. After the pretreatment with 5% O_2 in N_2 (50 mL min^{-1}) at 500 °C for 1 h and then cooling down to the desired temperature for the NO_x sorption, a gas mixture of 800 ppm NO and 5% O_2 balanced with N_2 passed through the loaded catalyst at a space velocity of 50,000 h^{-1}. An on-line chemi-luminescence NO_x analyzer (Model 42i-HL, Thermo Scientific) was used to determine the concentration of NO, NO_2 and NO_x. The duration of the NSC measurement for each catalyst was 30 min.

The NO temperature programmed desorption (NO-TPD) experiments were conducted with the same apparatus as the NSC measurements. 0.1 g of the catalyst was pretreated in 5% O_2/N_2 (50 mL min^{-1}) at 500 °C for 1 h, and then exposed in 800 ppm NO/5% O_2 balanced with N_2 for 1 h with a flow rate of 80 mL min^{-1} at 300, 400 or 500 °C, and then the reactor temperature decreased to room temperature with the same gas atmosphere, followed by purging the sample with N_2 flow until the NO_x concentration was below 15 ppm. Thereafter, the catalyst was heated to 700 °C at a rate of 10 °C min^{-1} and the flow rate of the carrier gas N_2 was 20 mL min^{-1}.

3. Results and discussion

3.1. Formation process of the $BaFeO_{3-x}$ catalyst

The thermal analysis profiles of the xerogel precursor of the $BaFeO_{3-x}$ catalyst are presented in Fig. 1. Below 100 °C, a small and broad DTG peak with an endothermic process was observed,

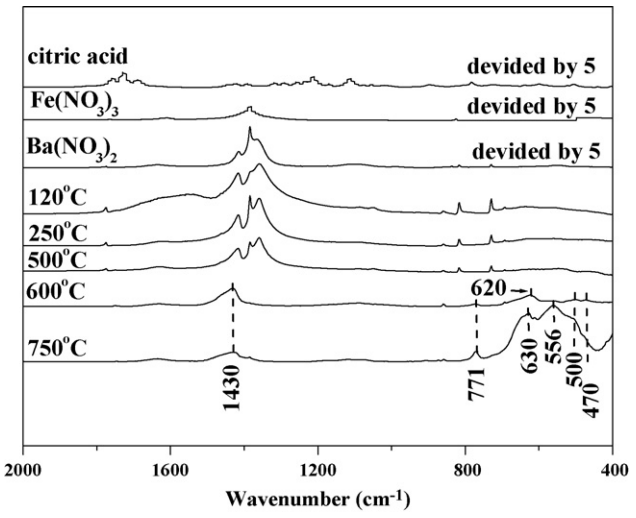

Fig. 2. FT-IR spectra of the xerogel precursor calcined at different temperature for 6 h.

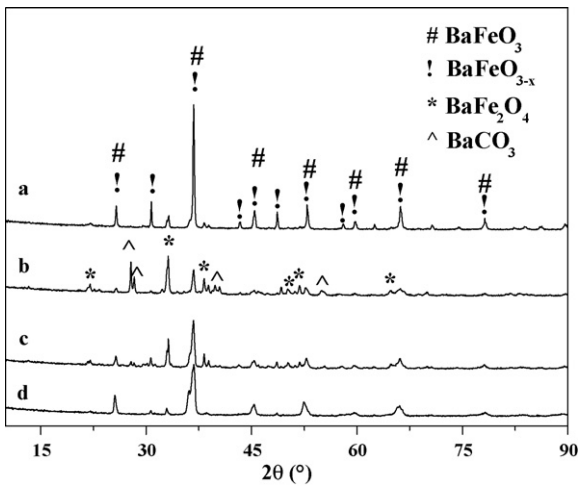

Fig. 3. XRD patterns of the catalysts (a) Ba–Fe–750F; (b) Ba–Fe–750S; (c) Ba–Fe–850S; and (d) Ba–Fe–950S.

which was correlated to the free water in the precursor by deliquescence. Between 135 and 280 °C, an endothermic peak of DTA was found following the mass loss of 28.3%. It was due to the chemically combined water in the xerogel precursor. With the increase of calcination temperature, a strong exothermic process occurred from 290 to 370 °C with the mass loss of 22.4%, which was derived from the citric acid combustion. Thereafter, the mass of the sample became stable until 498 °C that a shoulder DTG peak ranged from 498 to 620 °C, and centered at 573 and 602 °C appeared. At the same time, an endothermic process with the similar shape as the trend of the DTG profile on the DTA profile occurred, and the mass of the sample lost about 13.5%. This process was very complexed involving the carbonate decomposition, the nitrate from the salt sources decomposition, and some solid state reactions to form the spinel and perovskite species.

To clarify the formation process of the $BaFeO_{3-x}$ perovskite catalyst, the FT-IR spectra of the xerogel precursor, calcined at 120, 250, 500, 600, or 750 °C for 6 h in continuous air flow, are shown in Fig. 2. For the standard $Fe(NO_3)_3$ sample, only the vibration bond of nitrate at 1383 cm^{-1} was observed. Very strangely, there was no obviously vibration bond of the standard citric acid was found on the FT-IR profiles of the xerogel precursors. It might be due to the strong interaction between citric acid and water in the precursor, and, also, the formation of the coordinated complex between metal ions and citric acid. For the precursor calcined at 120, 250, and 500 °C, the bonds at 1414, 1383, 1356, 815, and 730 cm^{-1} were well matched with the standard $Ba(NO_3)_2$ material, indicating that even at 500 °C barium was still in the form of nitrate. At 120 °C, the broad bond from 1486 to 1770 cm^{-1} was due to the combined water as evidenced by the TG results in Fig. 1, and it disappeared at the higher calcination temperature. Moreover, the intensity of the nitrate vibration bonds decreased a little after the calcination temperature increased from 250 to 500 °C because of the partial decomposition of nitrate. When the calcination temperature increased to 600 °C, the nitrate species were completely decomposed so that the nitrate vibration bonds disappeared on the FT-IR spectra. Simultaneously, several new vibration bonds appeared at 1430, 771, 620, 500, and 470 cm^{-1}. The bond at 1430 cm^{-1} was related to the vibration bond of carbonate, while the others belonged to the characteristic vibration bonds of the spinel species [20]. When the calcination temperature reached 750 °C, two strong vibration bonds at 630 and 556 cm^{-1}, ranged from 470 to 750 cm^{-1}, were observed, which was due to the stretching vibration of the Fe–O bond in the octahedron cage FeO_6 at the B sites of the perovskite $BaFeO_3$ structures [20,21]. Here, the intensity of the vibration bonds of both the perovskite species and the spinel species was strengthened especially for the perovskite species. Moreover, the bond at 1430 cm^{-1} still remained, indicating the existence of carbonate in the Ba–Fe–750F catalyst after 750 °C calcination. These FT-IR results were coincided with the previous TG results that the nitrate decomposition, and the spinel and the perovskite formation occurred at above 500 °C. The high calcination temperature, especially higher than 600 °C, was favorable for the perovskite formation.

The XRD patterns and the BET surface area of the catalysts calcined at the various temperatures in air with or without flow are depicted in Fig. 3 and Table 1, respectively. In Fig. 3(a), it clearly shows that the $BaFeO_3$ (PDF number: 75-0426) and $BaFeO_{3-x}$ phases (PDF number: 70-0034 and 70-1321) were formed on the Ba–Fe–750F catalyst after the xerogel precursor calcined in the flowing air at 750 °C, and some weak diffraction peaks of the spinel $BaFe_2O_4$ phase (PDF number: 70-2468) was still observed demonstrating that the perovskite phases were the main the components. Nevertheless, no diffraction peak attributed to $BaCO_3$ phase was detected, which disagreed with the FT-IR results in Fig. 2. It is because the small amount of remnant carbonate might be well dispersed on the catalyst so that it was hardly detected from the XRD characterization. The diffraction peak at 30.6° was corresponding to the characteristic diffraction peak of the $BaFeO_{3-x}$ ($x = 0.27$ and 0.33) phases, indicating that a large amount of the defective perovskite species was formed here.

For comparison, the XRD pattern of the Ba–Fe–750S catalyst is presented in Fig. 3(b). The diffraction peaks belonging to perovskite (PDF number: 75-0426, 70-0034, and 70-1321), spinel (PDF number: 70-2468) and carbonate phases (PDF number: 71-2394) were observed, and the intensity of the diffraction peaks of the perovskite phases was much weaker than that of the later two phases. Here, CO_2 derived from citric acid combustion in static air was more difficultly released out of the muffle furnace than that in flowing air, which inhibited the perovskite formation. With the increase of the calcination temperature to 850 (Fig. 3(c)) and 950 °C (Fig. 3(d)), the

Table 1
The BET surface area and the NO_x storage capacity (NSC) at 400 °C of the catalysts.

Temperature	BET surface area ($m^2\ g^{-1}$)	NSC ($\mu mol\ g^{-1}$)
Ba–Fe–750F	6.0	333.5
Ba–Fe–750S	6.8	817.0
Ba–Fe–850S	5.9	575.6
Ba–Fe–950S	2.6	222.9

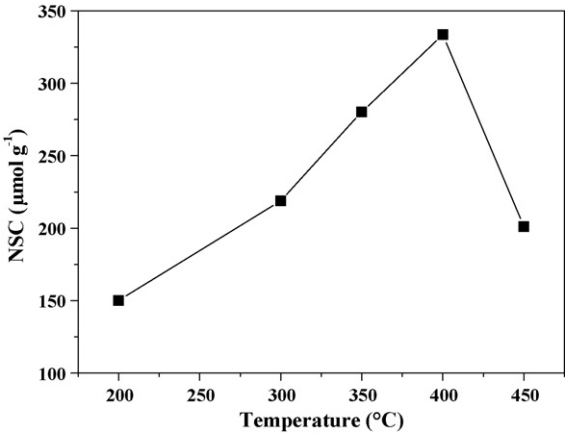

Fig. 4. NSC of the Ba–Fe–750F catalyst.

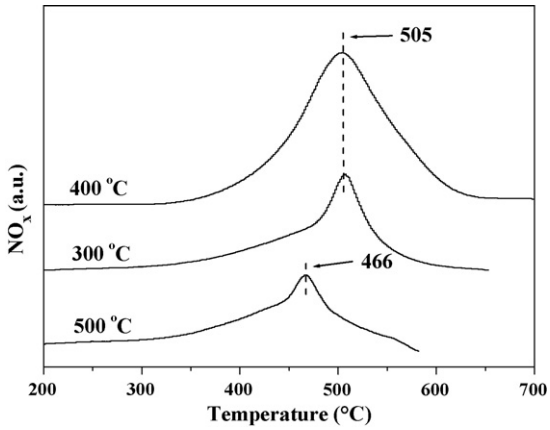

Fig. 5. NO-TPD spectra of the Ba–Fe–750F catalyst at various NO_x sorption temperature.

intensity of the diffraction peaks of the $BaCO_3$ and $BaFe_2O_4$ phases became weaker and weaker, and the diffraction peak of the $BaCO_3$ in the Ba–Fe–950S catalyst, calcined at 950 °C, even disappeared. Contrarily, the intensity of the diffraction peaks of the perovskite phases became stronger and stronger.

Here, a possible reaction route for the perovskite formation was proposed. Briefly, the spinel phase was formed at above 600 °C as evidenced by the previous FT-IR results, and the $BaCO_3$ phase decomposed gradually to BaO with the increasing of calcination temperature. BaO might react with the spinel phase to form the perovskite phases at the high calcination temperature:

$$BaCO_3 \rightleftharpoons BaO + CO_2 \quad (1)$$

$$BaO + BaFe_2O_4 + (1/2 - x)O_2 \rightleftharpoons 2BaFeO_{3-x}, \quad (0.5 > x > 0) \quad (2)$$

In Eq. (1), it is obvious that the presence of CO_2 would hinder the $BaCO_3$ decomposition to BaO, and, consequently, the perovskite formation in Eq. (2). It well explains the XRD results that, for the catalyst calcined in flowing air, the perovskite phases could be easily formed at 750 °C because CO_2 produced from citric acid combustion was purged away from the pipe furnace by air flow accelerating the proceeding of the reactions in Eqs. (1) and (2). On the other hand, the $BaCO_3$ decomposition was an endothermic reaction, and it could be promoted to produce BaO through calcination at high temperature by thermodynamic force. Thereafter, Eq. (2) was synergistically enhanced to form the perovskite species. So, the perovskite phases became the main components only on the Ba–Fe–950S catalyst among the catalysts without air purging due to its high calcination temperature.

Although the perovskite phases were the main components for both the Ba–Fe–750F and the Ba–Fe–950S catalysts, a bigger BET surface area was achieved for the former one as observed in Table 1, due to the lower calcination temperature.

3.2. NO_x storage process

The influence of the NO_x storage temperature to the NSC of the Ba–Fe–750F catalyst is displayed in Fig. 4. The NSC gradually increased following the increase of the storage temperature, and reached the maximum at 400 °C, i.e. 333.5 μmol g^{-1}. When the storage temperature was above 400 °C, the NSC dropped sharply. This result was in good agreement with our previous study [6] that the optimized NO_x storage temperature was 400 °C over the Pt/Ba–Al–O catalyst. Below 400 °C, NO_x was captured and stored from gas phase, and the amount of the stored NO_x increased over the catalyst following the increase of the NO_x sorption temperature [4,6]. However, the stored NO_x was unstable. It decomposed and released from the catalyst at above 400 °C [4,6]. Therefore, a volcano-like curve was presented during the NSC test. Moreover, the NSC of the perovskite catalysts adsorbing NO_x at 400 °C was compared in Table 1. The NSC of the Ba–Fe–750S catalyst possessed the much bigger NSC than that of the Ba–Fe–750F catalyst. It was due to the existence of the large amount of carbonate on the Ba–Fe–750S catalyst (Fig. 1), which would induce a poor sulfur resistance.

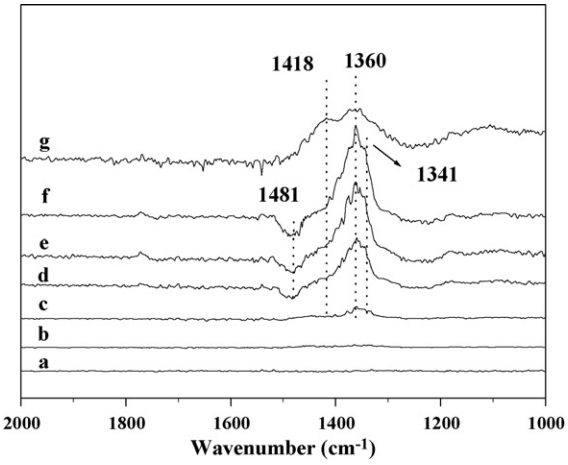

Fig. 6. *In situ* DRIFTS spectra of the Ba–Fe–750F catalyst (a-f), and the Ba–Fe–950S catalyst (g) with the different sorption period in 800 ppm NO_x/5% O_2 flow: (a) 1 min, (b) 5 min, (c) 10 min, (d) 20 min, (e) 40 min, and (f and g) 60 min.

Fig. 5 presents the NO-TPD spectra of the Ba–Fe–750F catalyst after NO_x sorption in 800 ppm/5% O_2 at 300, 400 or 500 °C for 1 h. The NO_x desorption area of the catalyst, exposed in NO_x and O_2 at 400 °C, was the biggest among three NO_x sorption conditions, which was coincided with the NSC results in Fig. 4 that the optimized NO_x sorption temperature was around 400 °C. Very interestingly, the tiptop of the NO_x desorption peak after NO_x sorption at 300 and 400 °C was about 505 °C, while the tiptop of the NO_x desorption peak after the NO_x sorption at 500 °C decreased to 466 °C. This shift of the NO_x desorption peak to low temperature was because the formed barium nitrate was unstable at 500 °C leading to the decomposition and the release of the stored nitrate. Accordingly, it possessed the smallest NO_x desorption area.

To investigate the NO_x storage behavior of the perovskite catalyst, the *in situ* DRIFTS spectra of the Ba–Fe–750F and Ba–Fe–950S catalysts in 800 ppm NO and 5% O_2 flow at 400 °C for the different sorption period are depicted in Fig. 6. The bond at 1341 cm^{-1} can be attributed to the monodentate nitrate over barium [22,23], while

the bonds at 1360 and 1418 cm^{-1} are correlated to the N-bounded nitrate [14,15]. Here, NO_x is directly binded with barium in the form of O–Ba–NO_2 due to the oxygen vacancies existing on the ABO_3 perovskite structures. As seen in Fig. 6, the major stored nitrate species for the perovskite catalysts was the N-bounded nitrate. The nitrogen atom was directly binded with barium atom. Therefore, the defective structure of the perovskites, i.e. oxygen atom vacancy, was beneficial for the N-bounded nitrate formation.

For the Ba–Fe–750F catalyst, the intensity of the nitrate bond was very weak at the beginning until the NO_x sorption was prolonged for 10 min (Fig. 6a–c). After the NO_x sorption for more than 20 min, a negative bond at around 1481 cm^{-1}, and two positive bonds at 1360 and 1341 cm^{-1} were clear observed. In our previous study, the similar negative bond attributed to the elimination of carbonate at 1466 cm^{-1} was evidenced during the NO_x sorption over the Pt/$BaCO_3$–Al_2O_3 catalyst [24]. The existence of carbonate on the Ba–Fe–750F catalyst has been confirmed by our FT-IR results in Fig. 2. Since the Ba–Fe–750F catalyst was calcined at 750 °C for 6 h much higher than that of the NO_x sorption temperature (400 °C), the appearance of this negative bond at 1481 cm^{-1} should be correlated to the direct transformation from carbonate to nitrate instead of the decomposition of carbonate to BaO and CO_2. The shift to the higher wavenumber in the present study (1481 cm^{-1}) than that in the previous report (1466 cm^{-1}) [24] may be due to the positive overlap of the nitrate bonds at 1418 cm^{-1}, correlating to the N-bounded nitrates. It indicates that, after the NO_x sorption, the N-bounded nitrate and monodentate nitrate were formed over the Ba–Fe–750F catalyst, simultaneously. For each profile in Fig. 6(a–f), the intensity of the N-bounded nitrate was always higher than that of the monodentate nitrate. With the prolonged NO_x sorption period, the intensity of the vibration bonds belonging to both nitrate and carbonate was strengthened indicating more NO_x was stored over the Ba–Fe–750F catalyst.

Here, the *in situ* DRIFTS experiment of the Ba–Fe–950S catalyst was also carried out to compare with the Ba–Fe–750F catalyst in Fig. 6(g). No bond belonging to carbonate was found on the profile, while the strong bonds ascribed to N-bounded nitrate at 1418 and 1360 cm^{-1} were clearly determined. It was in good agreement with the previous XRD results in Fig. 3 that no carbonate remaining on this catalyst. Comparison with the DRIFTS spectra of the Ba–Fe–750F catalyst, the absence of the monodentate nitrate bond in Fig. 6(g) indicates that the monodentate nitrate formed in Fig. 6(c–f) might be due to the transformation of carbonate to nitrate, while the N-bounded nitrate was corresponding to the nitrate formed on perovskite in Fig. 6(c–g). Therefore, two kinds of active sites might contribute to NO_x storage over the Ba–Fe–750F catalyst. One was the remnant carbonate transforming to monodentate nitrate. The other was that NO_x stored directly on the A site Ba in the ABO_3 perovskite structure through forming N-bounded nitrate in the form of O–Ba–NO_2.

4. Conclusions

Perovskite phase could be synthesized from a solid state process that $BaCO_3$ decomposed to BaO, which then reacted with the spinel species to produce perovskite. Here, the $BaCO_3$ decomposition played a key role for the perovskite formation, which could be enhanced by purging with air flow to remove the produced CO_2 out of the pipe furnace or by thermodynamical decomposing carbonate at high calcination temperature.

During NO_x sorption, the optimized NSC, i.e. 333.5 μmol g^{-1}, was achieved at 400 °C and the stored NO_x became unstable and released at high sorption temperature. Moreover, two kinds of the NO_x storage sites existed on the Ba–Fe–750F catalyst, i.e. the remnant carbonate transforming to monodentate nitrate, and the A site Ba in the ABO_3 perovskite structure directly binded with NO_x forming N-bounded nitrate.

Acknowledgements

The financial aids from the “863 Program” of the Ministry of Science & Technology of China (No. 2008AA06Z323), the National Natural Science Foundation of China (No. 20806056), the Natural Science Foundation of Tianjin (No. 09ZCGHHZ00400), and the Doctoral Fund of Ministry of Education of China (No. 200800561002) are greatly appreciated. This work is also financially supported by the Program for New Century Excellent Talents in University of China (NCET-07-0599), and the Cheung Kong Scholar Program for Innovative Teams of the Ministry of Education (No. IRT0641).

References

[1] J. Kašpar, P. Fornasiero, N. Hickey, Catal. Today 77 (2003) 419.
[2] N. Takahashi, H. Shinjoh, T. Iijima, T. Suzuki, K. Yamazaki, K. Yokota, H. Suzuki, N. Miyoshi, S. Matsumoto, T. Tanizawa, T. Tanaka, S. Tateishi, K. Kasahara, Catal. Today 27 (1996) 63.
[3] E. Fridell, H. Persson, B. Westerberg, L. Olsson, M. Skoglundh, Catal. Lett. 66 (2000) 71.
[4] S. Roy, A. Baiker, Chem. Rev. 109 (2009) 4054.
[5] X. Li, M. Meng, P. Lin, Y. Fu, T. Hu, Y. Xie, J. Zhang, Chem. Eng. Res. Des. 80 (2002) 190.
[6] X. Li, M. Meng, P. Lin, Y. Fu, T. Hu, Y. Xie, J. Zhang, Top. Catal. 22 (2003) 111.
[7] J. Yu, X. Wang, L. Li, Z. Hao, Z. Xu, Adv. Funct. Mater. 17 (2007) 3598.
[8] J. Yu, Y. Tao, C. Liu, Z. Hao, Z. Xu, Environ. Sci. Technol. 41 (2007) 1399.
[9] X. Li, P. Vernoux, Appl. Catal. B 61 (2005) 267.
[10] A. Lucas-Consuegra, Á. Caravaca, P. Sánchez, F. Dorado, J.L. Valverde, J. Catal. 259 (2008) 54.
[11] J. Liu, Z. Zhao, C. Xu, A. Duan, G. Jiang, J. Phys. Chem. C 112 (2008) 5930.
[12] H. Wang, Z. Zhao, P. Liang, C. Xu, A. Duan, G. Jiang, J. Xu, J. Liu, Catal. Lett. 124 (2008) 91.
[13] S. Hodjati, K. Vaezzadeh, C. Petit, V. Pitchon, A. Kiennemann, Appl. Catal. B 26 (2000) 5.
[14] S. Hodjati, C. Petit, V. Pitchon, A. Kiennemann, Appl. Catal. B 27 (2000) 117.
[15] S. Hodjati, C. Petit, V. Pitchon, A. Kiennemann, Appl. Catal. B 30 (2001) 247.
[16] K. Yamazaki, T. Suzuki, N. Takahashi, Appl. Catal. B 30 (2001) 459.
[17] M. Casapu, J.D. Grunwaldt, M. Maciejewski, A. Baiker, R. Hoyer, M. Wittrock, S. Eckhoff, Catal. Lett. 120 (2008) 1.
[18] M. Casapu, J.D. Grunwaldt, M. Maciejewski, A. Baiker, S. Eckhoff, U. Göbel, M. Wittrock, J. Catal. 251 (2007) 28.
[19] X. Li, J. Chen, P. Lin, M. Meng, Y. Fu, J. Tu, Q. Li, Catal. Commun. 5 (2004) 25.
[20] Y. Yang, Y. Jiang, Y. Wang, Y. Sun, J. Mol. Catal. A 270 (2007) 56.
[21] J. Miao, L. Li, Y. Song, D. Xu, Z. Lu, W. Su, Mater. Chem. Phys. 62 (2000) 226.
[22] C. Sedlmair, K. Seshan, A. Jentys, J.A. Lercher, J. Catal. 214 (2003) 308.
[23] P.T. Fanson, M.R. Horton, W.N. Delgass, J. Lauterbach, Appl. Catal. B 46 (2003) 393.
[24] J. Luo, M. Meng, X. Li, Y. Zha, Mircopor. Mesopor. Mater. 113 (2008) 277.